JACS
JOURNAL OF THE AMERICAN CHEMICAL SOCIETY
Article
pubs.acs.org/JACS

Cellular Toxicity Induced by the Photorelease of a Caged Bioactive Molecule: Design of a Potential Dual-Action Ru(II) Complex

Mark A. Sgambellone,[†] Amanda David,[‡] Robert N. Garner,[§] Kim R. Dunbar,*[,‡] and Claudia Turro*[,†]

[†]Department of Chemistry and Biochemistry, The Ohio State University, Columbus, Ohio 43210, United States
[‡]Department of Chemistry, Texas A&M University, College Station, Texas 77843, United States
[§]Department of Chemistry, University of the Incarnate Word, San Antonio, Texas 78209, United States

Supporting Information

ABSTRACT: The series $[Ru(tpy)(CH_3CN)_3]^{2+}$ (**1**), *cis*-$[Ru(tpy)(CH_3CN)_2Cl]^{+}$ (**2**), and $[Ru(tpy)(5CNU)_3]^{2+}$ (**3**), where tpy = 2,2′:6′,2″-terpyridine and 5CNU = 5-cyanouracil, was synthesized, and their photochemical properties were investigated for use as potential photodynamic therapy (PDT) agents. When irradiated with visible light, **1**−**3** exhibit efficient exchange of the axial CH_3CN or 5CNU ligand with H_2O solvent molecules. Complexes **1**−**3** also exhibit photoinitiated binding to DNA when irradiated with $\lambda_{irr} \geq 395$ nm light, and DNA binding can be accessed for **2** with $\lambda_{irr} > 645$ nm, well within the PDT window. Since **3** binds DNA and simultaneously releases biologically active 5CNU, it has the potential to be a dual-action therapeutic agent. Indeed, **3** is cytotoxic upon irradiation with visible light, whereas **1** is not under similar experimental conditions. The lack of toxicity imparted by **1** is explained by the exchange of only one CH_3CN ligand in the complex under the irradiation conditions used for the cellular studies. Strategies are being sought to increase the quantum yields of ligand exchange and the cellular penetration of these compounds.

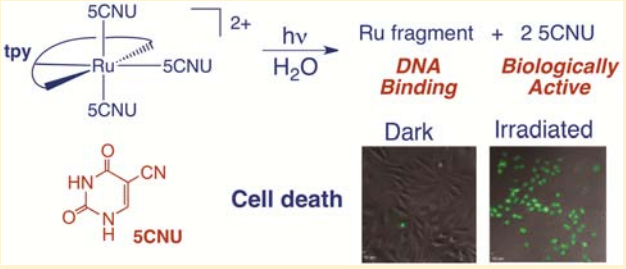

INTRODUCTION

The success of cisplatin, *cis*-$Pt(NH_3)_2Cl_2$, as an antitumor agent has led to the investigation of numerous transition metal compounds for potential use as chemotherapy agents.[1,2] Other platinum(II) complexes, such as carboplatin, *cis*-diammine-1,1′-cyclobutane dicarboxylate platinum(II), oxaliplatin, and *trans*-L-diaminocyclohexaneoxalatoplatinum(II), are currently in use to treat colorectal, ovarian, lung, and head and neck cancers.[1,3,4] Ruthenium compounds have shown promise as potential alternatives to platinum complexes,[2] and two ruthenium complexes have entered clinical trials as potential anticancer drugs. NAMI-A, [ImH][*trans*-$RuCl_4(DMSO)(Im)$], where Im = imidazole, DMSO = dimethylsulfoxide, exhibits antimetastatic behavior along with antitumor activity.[2] KP1019, [InH][*trans*-$RuCl_4(In)_2$], where In = indazole, shows signs of promoting apoptosis and exhibits activity in tumors that are resistant to other chemotherapy agents.[2] Although these complexes are currently undergoing clinical trials, severe side effects stemming from their low selectivity represents an important drawback.[1−5]

A promising strategy for controlling the selectivity of chemotherapy agents is to activate the drug with light, a field known as photodynamic therapy (PDT), such that the affected area can be irradiated selectively.[6−8] We previously showed that *cis*-$[Rh_2(\mu\text{-}O_2CCH_3)_2(CH_3CN)_6]^{2+}$ covalently binds to double-stranded DNA (ds-DNA) when irradiated with visible light ($\lambda_{irr} \geq 455$ nm). A 34-fold increase in toxicity toward Hs-27 human skin cells was observed when the complex was irradiated for 30 min with visible light, as compared to the same time period in the dark.[9] Complexes of the type $[Ru(bpy)_2L_2]^{2+}$, where bpy = 2,2′-bipyridine and L = NH_3, CH_3CN, thioethers, and 5-cyanouracil (5CNU), have also been shown to bind to ds-DNA upon irradiation.[10−12] Other caged Ru(II) complexes that release bioactive molecules upon irradiation have also been reported.[13,14] It is important to note that ligands bound to the metal through a nitrile, such as CH_3CN and 5CNU, display a notably greater ligand exchange quantum yield, Φ, as compared to other ligands.[12−16]

An important aspect of PDT is that the drug absorb in the PDT window, 600−850 nm.[17] The absorption spectrum of $[Ru(tpy)_2]^{2+}$, where tpy = 2,2′:6′,2″-terpyridine, exhibits a lower energy singlet metal-to-ligand charge-transfer (^{1}MLCT) absorption as compared to $[Ru(bpy)_3]^{2+}$ owing to the increased π-conjugation and the decrease in molecular symmetry in the former. In addition to red-shifting the ^{1}MLCT absorption maximum, Ru(II) complexes possessing tpy ligands have been shown to bind to 9-ethylguanine,[18] and $Ru(tpy)Cl_3$ exhibits significantly greater cytotoxicity than $Ru(bpy)_2Cl_2$.[19]

In the present work, $[Ru(tpy)(CH_3CN)_3]^{2+}$ (**1**), *cis*-$[Ru(tpy)(CH_3CN)_2Cl]^{+}$ (**2**), and $[Ru(tpy)(5CNU)_3]^{2+}$ (**3**) were synthesized and their photochemistry and photoinduced DNA binding investigated (Figure 1a). The free 5CNU molecule exhibits biological activity of its own through inhibition of pyrimidine catabolism.[20] The chemotherapy agent 5-fluorouracil,

Received: May 7, 2013
Published: July 2, 2013

   dx.doi.org/10.1021/ja4045604 | J. Am. Chem. Soc. 2013, 135, 11274−11282

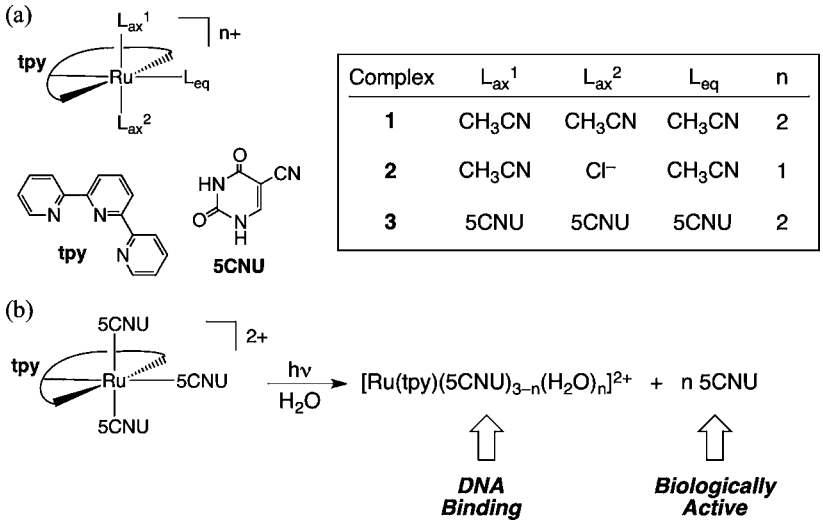

Complex	L_{ax}^1	L_{ax}^2	L_{eq}	n
1	CH_3CN	CH_3CN	CH_3CN	2
2	CH_3CN	Cl^-	CH_3CN	1
3	5CNU	5CNU	5CNU	2

Figure 1. (a) Schematic representation of the molecular structures of **1**−**3**, tpy, and 5CNU, and (b) photorelease of a metal complex able to bind DNA and of the biologically active 5CNU molecule through irradiation with visible light in water.

structurally related to 5CNU, has been in use for over 20 years for the treatment of malignancies including colorectal and breast cancers.[21] When 5CNU is introduced as a ligand in a complex that can undergo photoinduced binding to DNA, the resulting molecule has the potential to act as a dual-action phototherapeutic agent.[12,20] This concept is illustrated in Figure 1b, showing the release of active species upon irradiation that can achieve cell death via different mechanisms. Density functional theory (DFT) calculations were used to aid in the understanding of the electronic structure of the complexes. In general, the results show that **2** is able to bind to DNA when irradiated with light in the PDT window, but that **3** exhibits significantly greater toxicity when irradiated with visible light.

EXPERIMENTAL SECTION

Materials. The ligand 2,2′:6′,2″-terpyridine (tpy), sodium phosphate, gel loading buffer (0.05% (w/v) bromophenol blue, 40% (w/v) sucrose, 0.1 M EDTA (pH = 8.0), 0.5% (w/v) sodium lauryl sulfate), Tris base, Tris/HCl, and ethidium bromide were purchased from Sigma and used as received. The 5-cyanouracil (5CNU) reagent was purchased from Alfa Aesar, and pUC19 plasmid was purchased from Bayou Biolabs and purified using the QIAprep miniprep spin system from Qiagen. Cell culture reagents, *Sma*I, REact 4 buffer reagents, and Sytox Green were purchased from Invitrogen. The removal of *Sma*I was performed with the QIAquick gel extraction kit from Qiagen. $Ru(tpy)Cl_3$,[22] $[Ru(tpy)(CH_3CN)_3]^{2+}$ (**1**), and *cis*-$[Ru(tpy)(CH_3CN)_2Cl]^+$ (**2**) were prepared by procedures previously reported.[23]

$[Ru(tpy)(5CNU)_3]Cl_2$ (3). A sample of $Ru(tpy)Cl_3$ (0.114 mmol, 50 mg) was suspended in 10 mL of ethanol, resulting in a brown mixture to which $Ag(CF_3SO_3)$ (0.341 mmol, 88 mg) was added. The solution quickly turned purple and was filtered to remove AgCl after which time 5CNU (1.14 mmol, 156 mg) and 2 mL of H_2O were added. The mixture was refluxed under N_2 for 24 h, and the solvent was removed by evaporation. The crude product was dissolved in 10 mL of boiling H_2O, and a 5 mL aliquot of a saturated solution of NH_4PF_6 was added. The solution was placed in the freezer overnight to aid in precipitation of the product. The $[Ru(tpy)(5CNU)_3](PF_6)_2$ solid was collected and washed with cold H_2O and diethyl ether. The $[PF_6]^-$ anion was exchanged for Cl^- using an Amberlite column and eluted with methanol. Anal. Calcd for $[Ru(C_{15}H_{11}N_3)(C_5H_3N_3O_2)_3]Cl_2{\cdot}6.5H_2O$: C, 39.0%; H, 2.9%; N, 18.2%. Found: C, 39.3%; H, 3.3%; N, 18.1%. ^1H NMR (400 MHz) in D_2O δ ppm (splitting, integration): 7.80 (t, 2H) tpy, 7.97 (s, 2H) 5CNU axial, 8.24 (m, 3H) tpy, 8.50 (d, 4H) tpy, 8.69 (s, 1H) 5CNU equatorial, 9.10 (d, 2H) tpy.

Instrumentation. Electronic absorption measurements were performed on a Hewlett-Packard diode array spectrometer with HP 8453 Win System software. For steady-state photolysis experiments, a 150 W Xe lamp housed in a Milliarc compact arc lamp housing (PTI) and powered by a PTI model LPS-220 power supply was used; the irradiation wavelength was controlled with colored glass long-pass and band-pass filters (Newport and Thor Laboratories). ^1H NMR spectra were collected on a Bruker DRX-400 spectrometer, and electrochemical studies were performed on a BAS CV-50W voltammetric analyzer. Ethidium bromide stained gels were imaged on a Gel Doc 2000 (Biorad) transilluminator with Quantity One software.

Methods. The solutions for the photolysis experiments were deoxygenated by bubbling them with N_2 for 15 min prior to irradiation. Photosubstitution quantum yields were determined using ferrioxalate actinometry as previously described in detail.[24] Cyclic voltammetry measurements were performed using a three-electrode cell with a glassy carbon working electrode, a platinum wire auxiliary electrode, and a Ag/AgCl reference electrode using distilled CH_3CN containing 0.1 M tetra-*n*-butylammonium hexafluorophosphate as the supporting electrolyte. At the end of each experiment, a small amount of ferrocene (Fc) was added as an internal standard, and $E_{1/2}(Fc^{+/0})$ = 0.66 V vs NHE was used as a reference for calculating the oxidation and reduction potentials of each complex.[25]

Plasmid was linearized by incubating 50 units of *Sma*I with 10 μg of pUC19 plasmid and 10 μL of REact 4 buffer at 30 °C for 1 h followed by 10 min at 65 °C. The linearized DNA was separated from the enzyme using a QIAquick gel extraction kit. The concentration of plasmid DNA was determined from its absorption at 260 nm using an extinction coefficient of 6 600 M^{-1} cm^{-1} per base in accordance with the Qiagen protocol. The DNA mobility experiments were carried out using a 20 μL total sample volume in 0.5 mL transparent Eppendorf tubes containing 50 μM linearized pUC19 plasmid, 10 mM sodium phosphate buffer, and a concentration of metal complex that was varied as needed. Following irradiation or dark incubation, 4 μL of DNA gel loading buffer was added to each sample. The electrophoresis was carried out in 1× TBE buffer (TBE = tris-borate/EDTA, 0.09 M tris-borate, 0.002 M EDTA, pH = 8.3) using a 0.75% agarose gel and run at 92 V for 1 h. Staining was conducted after the electrophoresis by soaking the gel in a 0.5 μg/mL aqueous ethidium bromide solution followed by washing in water for 30 min.

Density functional theory calculations were performed using the Gaussian 09 program.[26] The B3LYP[27−29] functional along with the 6-31G* basis set for H, C, N, and O,[30] and the SDD energy-consistent pseudopotentials for Ru were used.[31] Geometries were fully optimized using the criteria of the respective programs. Orbital analysis was completed with GaussView.[32]

dx.doi.org/10.1021/ja4045604 | J. Am. Chem. Soc. 2013, 135, 11274−11282

Table 1. Absorption Maxima and Molar Extinction Coefficients, Ligand Exchange Quantum Yields, and Redox Potentials for 1−3, and Experimental (ΔE_{exp}) and Calculated (ΔE_{calc}) HOMO energies for 2 and 3 Relative to 1

complex	λ_{abs}/nm ($\varepsilon/\times10^3$ M^{-1} cm^{-1})[a]	λ_{em}/nm[b]	Φ_{Cl}[c]	Φ_{H_2O}[d]	$E_{1/2}$/V[e]	ΔE_{exp}/V[f]	ΔE_{calc}/V[g]
1	298 (31.0), 330 (17.8), 434 (4.0)	550, 596	0.040(1)	0.035(1)	+1.80, −1.20		
2	309 (27.8), 485 (4.0)	597, 655	0.12(1)	0.12(1)	+1.18, −1.30	0.62	0.66
3	306 (35.6), 330 (33.5), 420 (4.5)	562, 603	*h*	0.022(2)	+1.82, −1.18	0.02	0.13

[a]In H_2O, 298 K. [b]At 77 K in EtOH/MeOH (4:1, v/v). [c]For the formation of *trans*-$[Ru(tpy)(L)Cl_2]^+$ in CH_2Cl_2 with excess $(n\text{-}C_4H_9)_4NCl$ (λ_{irr} = 400 nm). [d]For the formation of *trans*-$[Ru(tpy)(L)(H_2O)_2]^{2+}$ (λ_{irr} = 400 nm). [e]Vs NHE in CH_3CN with 0.1 M $N(n\text{-}C_4H_9)_4PF_6$. [f]$\Delta E_{exp} = |E_{1/2}[\mathbf{1}]^{3+/2+} - E_{1/2}[complex]^{3+/2+}|$. [g]$\Delta E_{calc}$ = |HOMO(**1**) − HOMO(complex)|. [h]**3** is not soluble in CH_2Cl_2.

The HeLa cell line was obtained from the American Type Culture Collection, cell line CCL-2. HeLa cells were cultured in Dulbecco's modified Eagle medium, containing 10% fetal bovine serum (Life Technologies), 50 μg/mL gentamicin, 4.5 mg/mL glucose, and 4 mM L-glutamine (Invitrogen Life Technology). Cell cultures were incubated in a humidified atmosphere containing 5% CO_2 at 37 °C.

HeLa cells, at a concentration of 5000−10000 cell/μL, were harvested, 20 μL of cell solution was seeded in an 8-well sterile plate, and 180 μL of fresh medium was added to give a total volume of 200 μL. Cells were preincubated at 37 °C. After 48 h, the cell cultures were washed three times with sterile PBS, and the medium was replaced with 100 μL of L-15 medium containing each compound at the desired concentration. Plates were incubated for 2 h after which time they were irradiated for 1 h inside a UV/vis photoreactor LZC-4 (Luzchem Research, Inc.), equipped with 14 lamps (λ_{irr} > 400 nm). The 8-well sterile plates with 80% cell confluency in each well were placed on an inverted epifluorescence microscope (model IX81, Olympus Center Valley, PA). The microscope was equipped with a heating stage which was maintained at 37 °C. The microscope was configured with a spinning disk unit to perform both confocal and wide-field fluorescence microscopy. Images were captured with a Rolera-MGI Plus back-illuminated EMCCD camera (Qimaging, Surrey, BC, Canada). Imaging was performed using the fluorescence filter set for FITC (ex = 488 ± 10 nm, em = 520 ± 20 nm), and the fluorescence intensities of HeLa cells were measured with the SlideBook 4.2 software (Olympus, Center Valley, PA). After irradiation for 1 h, the cells were washed three times with sterile PBS, and the medium was replaced with 90 μL of L-15 medium, treated with 10 μL of a 20 μM SYTOX Green solution, and incubated for 10 min before imaging. SYTOX Green is cell-impermeable and exclusively stains cells with a compromised plasma membrane. Cells were imaged with a 20× objective.

Cell viability for compound **3** and free 5CNU was determined by establishing the ratio of dead cells to the total number of cells for each sample, and at least 1000 cells were counted in each experiment, all of which were performed in triplicate. Ten images were acquired in the green channel for each experiment. The total number of cells in an image was determined from the phase contrast image. The number of dead cells was determined by identifying cells containing a green fluorescent nucleus stained by SYTOX Green.

RESULTS AND DISCUSSION

Electronic Absorption, Emission, and Electrochemistry. The molecular structures of **1**−**3** are schematically depicted in Figure 1a, and their electronic absorption maxima exhibit the characteristic ππ* transitions localized on the tpy ligand at ~300 and ~330 nm (Table 1).[33] The ^{1}MLCT (metal-to-ligand charge transfer) $Ru(t_{2g})\rightarrow tpy(\pi^*)$ transitions in **1** and **2** are observed with maxima at 434 and 485 nm, respectively, which agree with a previous report.[23] The electronic absorption spectrum of the new complex, **3**, shown in Figure 2 exhibits a ^{1}MLCT peak with maximum at 420 nm. Complexes **1**−**3** are not emissive at 298 K, but luminescence was detected at 77 K in a EtOH/MeOH (4:1, v/v) glass (Table 1). The emission spectrum of **3** is displayed in Figure 2, and those of **1** and **2** are shown in Figure S1 (Supporting Information). The emission

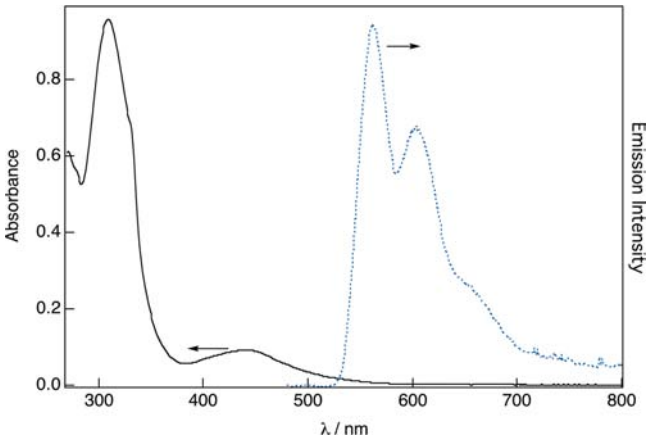

Figure 2. Electronic absorption spectrum (solid line) of **3** at 298 K and emission spectrum (dotted line) at 77 K in EtOH/MeOH (4:1, v/v).

spectra of **1**−**3** display the vibronic structure of each complex with spacing of 1403, 1483, and 1211 cm^{-1}, consistent with that previously reported for $[Ru(tpy)_2]^{2+}$ and other tpy-containing Ru(II) complexes whose emission is known to arise from the Ru→tpy ^{3}MLCT state.[34,35]

The oxidation and reduction potentials of **1**−**3** are listed in Table 1. The $Ru^{3+/2+}$ couples of **1** and **2** were determined to be +1.80 V and +1.18 V vs NHE, respectively, in CH_3CN and agree well with previous reports.[23] The oxidation potential of **3** was measured to be +1.82 V vs NHE, which is similar to that of **1** and those of other Ru(II) tpy complexes[23,34] and is therefore also assigned to the metal-centered $Ru^{3+/2+}$ couple. The relatively large difference in the oxidation potential of **2** as compared to those of **1** and **3** is expected to be due to the presence of the π-donating axial Cl^- ligand which destabilizes the Ru(dπ) orbitals and renders the metal complex more easily oxidized. This destabilization of the HOMO is also apparent in the calculated MO diagrams of the complexes as discussed in more detail below. The reduction potentials of **1** and **2** in CH_3CN at −1.20 and −1.30 V vs NHE, respectively, also agree well with previous reports and are assigned to the reduction of the tpy ligand.[34] Complex **3** exhibits a reduction event at −1.18 vs NHE assigned as a reduction of the tpy ligand based on a comparison to the electrochemical properties of **1** and **2**. It should be noted that an irreversible event at −0.88 V is observed for **3** when the electrochemistry is conducted in room light but which does not appear in the dark. This irreversible reduction is associated with a photoproduct which, although absent in the first cyclic voltammetry scan of free 5CNU ligand in CH_3CN (E_p = −1.21 V vs NHE), appears in subsequent scans (Figure S10).

Photochemistry. Irradiation of the ^{1}MLCT transition of **1** results in ligand exchange of bound acetonitrile ligands with solvent molecules or halides in solution, as previously reported.[23]

dx.doi.org/10.1021/ja4045604 | J. Am. Chem. Soc. 2013, 135, 11274−11282

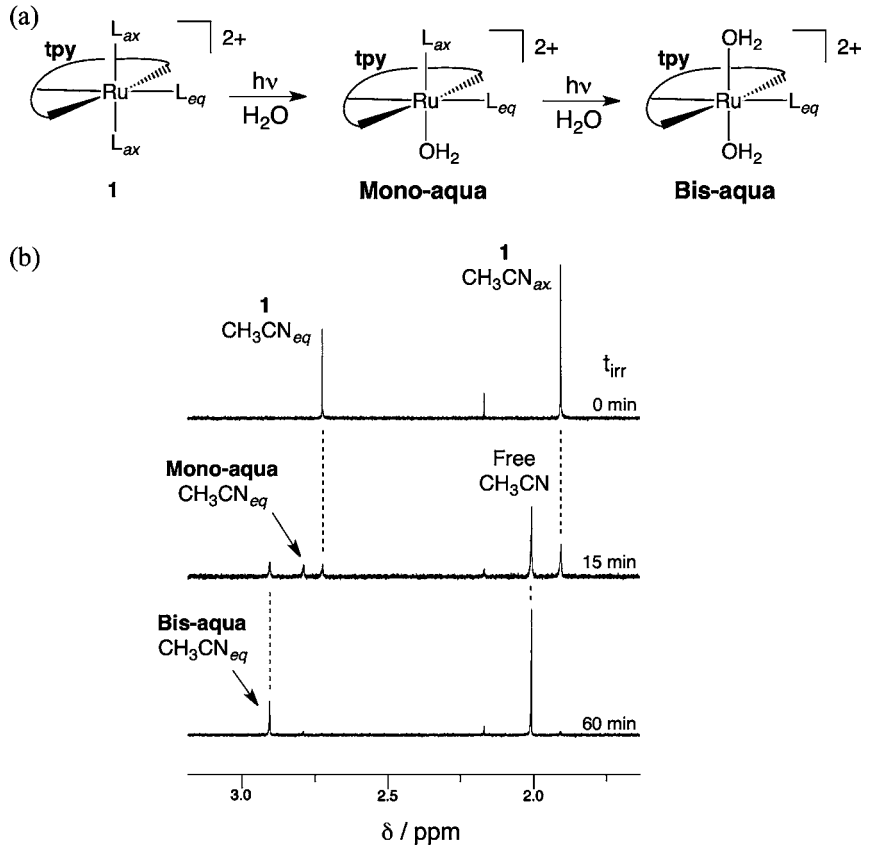

Figure 3. (a) Stepwise ligand exchange upon irradiation of **1** in H_2O and (b) changes to the ^{1}H NMR spectrum of **1** in D_2O as a function of irradiation time, t_{irr}.

A solution of 130 μM of **1** and 10 mM tetrabutylammonium chloride (TBACl) was irradiated with 400 nm light in CH_2Cl_2, and the changes to its electronic absorption were monitored as a function of irradiation time (Figure S2). The ^{1}MLCT transition of **1** at 434 nm decreases in intensity with the simultaneous increase in a peak with maximum at 485 nm (Figure S2). This shift of the ^{1}MLCT to lower energy is explained by the exchange of an acetonitrile ligand for a chloride anion, which results in a decrease of the ligand field splitting as the π-donor chloride ligand replaces the π-acceptor acetonitrile. This intermediate is therefore identified as *cis*-$[Ru(tpy)(CH_3CN)_2Cl]^+$ by the position of the peak at 485 nm, as previously reported.[23] Continued photolysis results in disappearance of the intermediate and an increase in intensity of a feature at 550 nm. The observation of two separate sets of isosbestic points at early and later photolysis times also indicates the formation and disappearance of an intermediate. Since the intermediate is a stable compound that can be isolated, the overall reaction is a sequential, two-photon process. The final product of the photolysis is *trans*-$Ru(tpy)(CH_3CN)Cl_2$, as is apparent from a comparison of the electronic absorption spectrum of the photoproduct of **1** to that of independently synthesized *trans*-$Ru(tpy)(CH_3CN)Cl_2$, which exhibits a small peak corresponding to the intermediate **2** at 485 nm (Figure S3). It should be mentioned that, during the synthesis of *cis*-$[Ru(tpy)(CH_3CN)_2Cl]^+$ and *trans*-$Ru(tpy)(CH_3CN)Cl_2$, no trace of the isomers *trans*-$[Ru(tpy)(CH_3CN)_2Cl]^+$ or *cis*-$Ru(tpy)(CH_3CN)Cl_2$ was detected, indicating that these species do not generally form.

It was previously demonstrated by Walsh and co-workers that the axial acetonitrile ligands of **1** are replaced by chloride ions upon irradiation, whereas the equatorial acetonitrile ligand positioned trans to the tpy ligand remains coordinated to the metal.[23] The difference in reactivity of axial and equatorial acetonitrile ligands can be explained by the trans effect since both acetonitrile and chloride have a stronger trans effect than pyridine. Therefore, the ligand positioned trans to the pyridine ring of tpy is less likely to be substituted. It should also be noted that it is necessary to deoxygenate the solution by bubbling with nitrogen prior to photolysis. In the presence of air, a different photolysis product is obtained. Since no ^{1}H NMR signals were detected for this product, it is most likely an oxidized paramagnetic ruthenium(III) compound. The ligand exchange quantum yield, $\Phi_{Cl}^{1\rightarrow4}$, for the overall formation of *trans*-$Ru(tpy)(CH_3CN)Cl_2$ (**4**) from **1** is 0.040(1), λ_{irr} = 400 nm, consistent with the reported values with 436 and 480 nm irradiation.[23] In the dark, no changes to the electronic absorption spectrum of **1** are observed when monitored for 24 h at 298 K (Figure S4a).

When **1** is irradiated in water, a decrease in the intensity of the ^{1}MLCT band is observed, with a concomitant increase of an absorption with a maximum at 475 nm (Figure S2b). The photolysis product is inconsistent with the formation of $[Ru(tpy)(H_2O)_3]^{2+}$, which absorbs with a maximum at 532 nm.[36] Based on earlier results that indicate lack of exchange of the acetonitrile ligand trans to the tpy ligand, the photoproduct may be ascribed to *trans*-$[Ru(tpy)(H_2O)_2(CH_3CN)]^{2+}$ (**Bis-aqua**). This overall process likely proceeds via the **Mono-aqua** intermediate as schematically depicted in Figure 3a, a point that was confirmed through the photolysis of **1** followed by ^{1}H NMR spectroscopy in D_2O as a function of irradiation time

dx.doi.org/10.1021/ja4045604 | J. Am. Chem. Soc. 2013, 135, 11274−11282

(Figure 3b). After 15 min of irradiation ($\lambda_{irr} \geq 395$ nm), the reactant peaks corresponding to the axial and equatorial acetonitrile ligands of **1**, at 1.91 and 2.72 ppm, respectively, decrease in intensity along with the formation of new peaks at 2.01, 2.79, and 2.90 ppm. The peak at 2.01 ppm is known to correspond to free acetonitrile in D_2O. Since the feature at 2.79 ppm decreases in intensity upon further irradiation, it is assigned to the equatorial acetonitrile of the intermediate, *cis*-$[Ru(tpy)(CH_3CN)_2(H_2O)]^{2+}$ (Figure 3a, **Mono-aqua**). The absorption at 2.90 ppm continues to increase in intensity for the duration of the experiment and is assigned as the equatorial acetonitrile of the **Bis-aqua** product, *trans*-$[Ru(tpy)(CH_3CN)(H_2O)_2]^{2+}$ (Figure 3). The peak corresponding to the axial acetonitrile ligands completely disappears, and the new free acetonitrile peak integrates to six hydrogen atoms, indicating that both axial acetonitrile ligands are exchanged during irradiation, whereas the resonance corresponding to the equatorial acetonitrile ligand of the photoproduct integrates to 3 hydrogen atoms, indicating that this ligand is not exchanged.

In the aromatic region of the ^{1}H NMR spectrum of **1**, the peak at 8.88 ppm shifts upfield by about 0.1 ppm early in the photolysis, corresponding to the formation of the **Mono-aqua** intermediate. Prolonged irradiation of the complex results in a further upfield shift of this peak by an additional 0.2 ppm, consistent with the formation of the final **Bis-aqua** product. The Φ_{H_2O} for the overall reaction is 0.035(1), and no changes to the electronic absorption spectrum of **1** are observed in the dark over 24 h at 298 K (Figure S4b).

Figure S5a depicts the photolysis of 250 μM of **2** and 10 mM of TBACl in CH_2Cl_2. It should be noted that complex **2** represents the intermediate in the photolysis of **1** to *trans*-$Ru(tpy)(CH_3CN)Cl_2$ (**4**) described above. Irradiation of **2** (λ_{irr} = 450 nm) results in the formation of *trans*-$Ru(tpy)(CH_3CN)Cl_2$ with $\Phi_{Cl}^{2\rightarrow4}$ = 0.12(1) as previously reported, where the axial CH_3CN ligand is exchanged but the equatorial CH_3CN remains bound to the metal.[23] Figure S3 depicts a comparison of the photoproduct to that of independently synthesized *trans*-$Ru(tpy)(CH_3CN)Cl_2$. The quantum yield for the formation of the final product **4** from **2**, $\Phi_{Cl}^{2\rightarrow4}$, is significantly larger than that measured for **1**, which may be explained by the fact that it is only a one-step process to the final product in **2** whereas the reaction is a two-step process in **1**. Based on the values of $\Phi_{Cl}^{1\rightarrow4}$ and $\Phi_{Cl}^{2\rightarrow4}$ and the sequential nature of the reaction, $\Phi_{Cl}^{1\rightarrow2}$ can be calculated to be 0.33(3).

The photolysis of **2** was followed by electronic absorption spectroscopy in H_2O (Figure S5b) and by ^{1}H NMR spectroscopy in D_2O, which resulted in the formation of the same photoproduct as for **1** (Figure 3a). For **2**, however, integration of the free CH_3CN after photolysis corresponds to 3 hydrogen atoms, as there is only one axial CH_3CN ligand that exchanges with D_2O. It should be noted that placement of **2** in H_2O or D_2O results in the exchange of the coordinated Cl^- anion for solvent, such that the starting material in these photochemical reactions is the **Mono-aqua** intermediate *cis*-$[Ru(tpy)(CH_3CN)_2(S)]^{2+}$ (S = H_2O, D_2O) and not **2**. This is apparent in the large shift in the absorption maximum of **2** when it is dissolved in water, from 485 nm in CH_2Cl_2 to 450 nm in H_2O. Such a change is consistent with the replacement of Cl^- with the stronger field ligand, H_2O. Moreover, this shift is not observed for **1**, with a maximum at 434 nm in both solvents. The quantum yield for product formation, Φ_{H_2O}, was measured to be 0.12(1). This value is greater than that measured for **1** because the photolysis reaction is a one-step process from the **Mono-aqua** intermediate to the **Bis-aqua** product for **2**, as compared to a two-step process for **1** (Figure 3a). No spectral changes occurred in the dark for **2** in the presence of Cl^- in CH_2Cl_2 or in water (Figure S6).

The $[PF_6]^-$ salt of **3** is insoluble in CH_2Cl_2 and acetone, which precluded photolysis experiments and the determination of Φ_{Cl} under conditions similar to those described above for **1** and **2**. The changes to the electronic absorption spectrum of **3** upon irradiation in H_2O are shown in Figure 4. The ^{1}MLCT

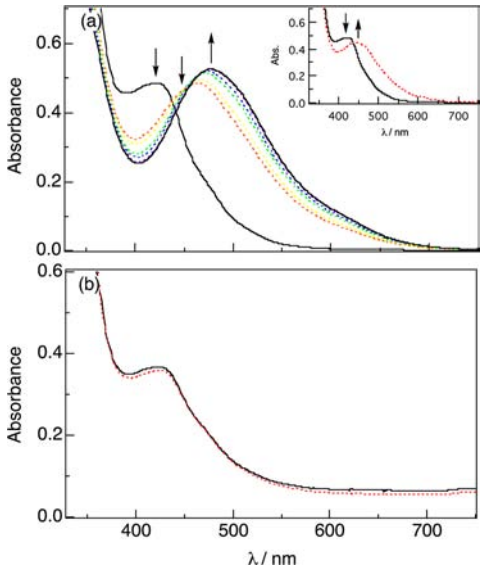

Figure 4. Changes to the electronic absorption in H_2O of (a) 100 μM **3** upon photolysis at t_{irr} = 0, 4, 6, 8, 10, 15 min. Inset: 0, 2 min ($\lambda_{irr} \geq$ 395 nm) and (b) 85 μM **3**; t_{dark} = 0, 24 h.

peak of **3** decreases in intensity after 1 min of irradiation with the simultaneous increase of a peak at ~450 nm (Figure 4a inset). By comparison to the photochemistry of **1**, this intermediate is assigned to the corresponding mono-aqua species, *cis*-$[Ru(tpy)(5CNU)_2(H_2O)]^{2+}$. Upon further irradiation, the absorption of the intermediate decreases in intensity and that of the final photoproduct increases, with a maximum at 475 nm (Figure 4). The photolysis of **3** was also followed by ^{1}H NMR spectroscopy (Figure 5), which shows that the axial 5CNU peak at 7.98 ppm disappears after 45 min of irradiation, with concomitant increase of a peak at 8.35 ppm known to correspond to free 5CNU in D_2O. Over the same time period, the peak assigned to equatorial 5CNU shifts from 8.70 to 8.75 ppm. Thus, as in the case of **1** and **2**, the equatorial 5CNU ligand is not photoactive and the final photoproduct is therefore assigned to *trans*-$[Ru(tpy)(5CNU)(H_2O)_2]^{2+}$. The Φ_{H_2O} for this reaction is 0.022(2), which is similar in magnitude to that of **1**. No reaction is observed in the dark as judged by monitoring the electronic absorption spectra for 24 h at 298 K (Figure 4b) or by ^{1}H NMR spectroscopy for 1 h at 298 K.

Electronic Structure Calculations. Density functional theory (DFT) calculations were performed to aid in the interpretation of the experimental data. The molecular orbital (MO) diagrams of **1**−**3** are shown in Figure 6. The LUMOs of the complexes, which are tpy(π^*) in character, were set to an equal energy because of the similar experimental values in the tpy localized reduction potential, and the HOMO of **1** was set to 0.0 eV as an arbitrary reference. The HOMO, HOMO-1, and

dx.doi.org/10.1021/ja4045604 | J. Am. Chem. Soc. 2013, 135, 11274−11282

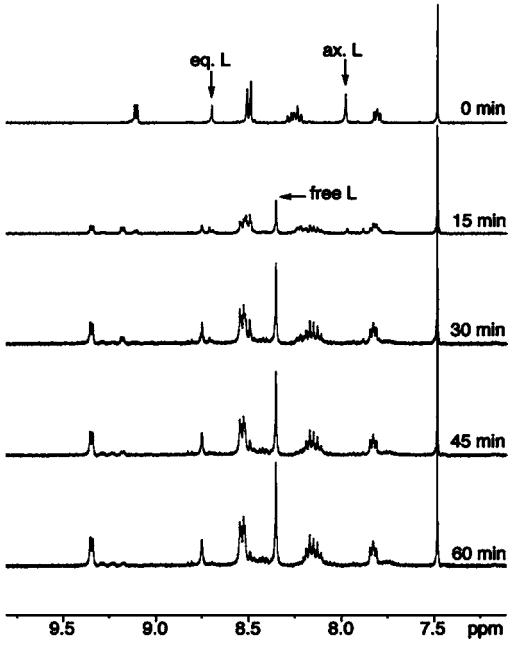

Figure 5. Changes to the ^{1}H NMR of **3** upon photolysis in D_2O at t_{irr} = 0, 15, 30, 45, 60 min ($\lambda_{irr} \geq 395$ nm), where L = 5CNU, ax. = axial, and eq. = equatorial.

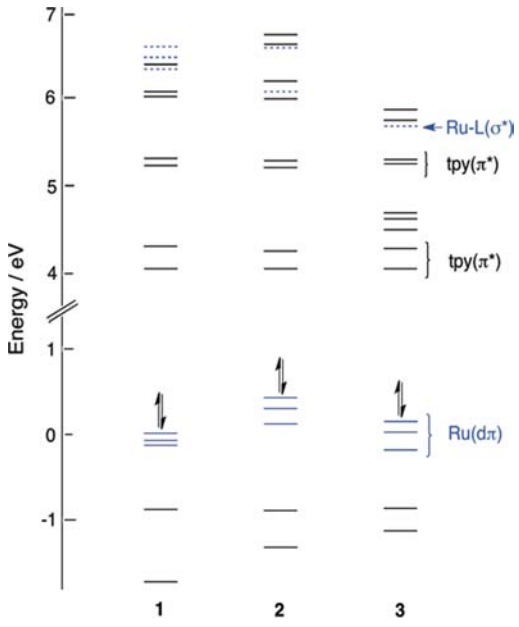

Figure 6. Molecular orbital diagrams of **1**−**3**, where Ru-L(σ^*) orbitals are denoted with dashed lines.

HOMO-2 of **1** and **3** are metal-based and represent the Ru(dπ) t_{2g}-type orbitals in a pseudo-octahedral environment. In **2**, the same orbitals are mostly metal-based, but the HOMO and HOMO-1 have significant π^* contribution from the chloride ion, a feature that explains the increase in energy of the HOMO and HOMO-1 relative to those of **1** and **3**, and as well as the red shift of the experimental ^{1}MLCT maximum. The calculated energy difference between the HOMO of **1** and **2**, ΔE_{calc}, is 0.66 V, which agrees well with the energy difference of the oxidation potentials between the two complexes, ΔE_{exp}, 0.62 V (Table 1). The HOMO-4 in each complex is tpy(π), as is the HOMO-5 of **1**. In **2** and **3**, however, the HOMO-5 is localized on the Cl^- and 5CNU ligands, respectively.

Each complex exhibits four unoccupied molecular orbitals that are tpy(π^*) in character at similar energies. These orbitals comprise the LUMO and LUMO+1 in each complex and the LUMO+2 and LUMO+3 in **1** and **2**. In **3**, the latter two MOs are calculated as the LUMO+5 and LUMO+6 (Figure 6). In **1**, the LUMO+4 and LUMO+5 are also tpy(π^*)-based, as is the LUMO+4 in **2**. The LUMO+2, LUMO+3, and LUMO+4 of **3** are localized on the 5CNU ligand. The LUMO+6, LUMO+8, and LUMO+9 of **1** can be described as Ru-L(σ^*) orbitals, where L = CH_3CN. The Ru-L(σ^*) orbitals are also observed in **2** as the LUMO+5 and LUMO+7, and in **3**, where L = 5CNU ligand, as the LUMO+7.

Population of the Ru-L(σ^*) orbitals is associated with the ligand field (LF) state that has been implicated in photoinduced ligand dissociation in Ru(II) complexes. Interestingly, the lowest energy Ru-L(σ^*) orbitals in **1**−**3** exhibit antibonding character to the axial ligands. Therefore, in addition to the trans effect, the presence of these orbitals provides an explanation for the observed exchange of axial ligands in these complexes. DFT calculations were also undertaken for the mono-aqua intermediates, *cis*-$[Ru(tpy)(CH_3CN)_2(H_2O)]^{2+}$ and *cis*-$[Ru(tpy)(5CNU)_2(H_2O)]^{2+}$. In both cases, the lowest energy unoccupied molecular orbital with Ru-L(σ^*) character corresponds to those associated with the remaining axial CH_3CN or 5CNU ligand, respectively. The trans effect would predict that the ligand across from the pyridine ring of tpy would labilize before the ligand trans to H_2O; however, as discussed earlier, it is the axial ligand trans to H_2O that is substituted. The calculations for the mono-aqua complexes indicate that the lowest energy Ru-L(σ^*) orbital has antibonding character between the metal and the remaining axial ligand, which is in accord with the preferential photodissociation of the second axial ligand.

Photoinitiated DNA Binding. Agarose gel electrophoresis has been used to demonstrate the covalent binding of cisplatin to double-stranded (ds) DNA, as well as the photoinitiated binding of other transition metal complexes to the double helix.[9−12,37] Mobility shift assays were undertaken to determine the ability of **1**−**3** to bind to ds-DNA when irradiated and were compared to experiments performed under similar conditions in the dark. In the gels presented in Figures 7, S7, and S8, lanes 1 and 8 are 1 kb DNA molecular weight standards and lanes 2 and 7 are controls showing 50 μM linearized pUC19 plasmid in the absence of any complex. Figures 7a and 7b show the complexes [**1**](Cl_2) and [**2**](PF_6), respectively, and their ability to decrease the mobility of 50 μM linearized plasmid when irradiated for 5 min with $\lambda_{irr} \geq 395$ nm light. The concentrations of lanes 3−6 are 1.0, 2.5, 5.0, and 10 μM, respectively. Complex **1** exhibits a slightly greater decrease in DNA mobility than **2** for the same complex concentrations, but this may be due to the difference in counterion. The mobility shift assay for **3** is shown in Figure 7c. Lanes 3−6 have greater concentrations, 5, 10, 25, and 50 μM, respectively, and a longer irradiation time, 15 min, as compared to the experiments with **1** and **2**, which is consistent with the lower ligand exchange quantum yield of **3** as compared to those of **1** and **2**. Control gels of the complexes incubated in the dark with DNA under similar conditions are shown in Figure S7, where no shift in the mobility is observed, indicating that light is required for DNA binding. The electronic absorption spectrum of **2** displays an extended tail to approximately 650 nm, such that excitation may be possible in the PDT window, 600−850 nm. Figure S8a

dx.doi.org/10.1021/ja4045604 | J. Am. Chem. Soc. 2013, 135, 11274−11282

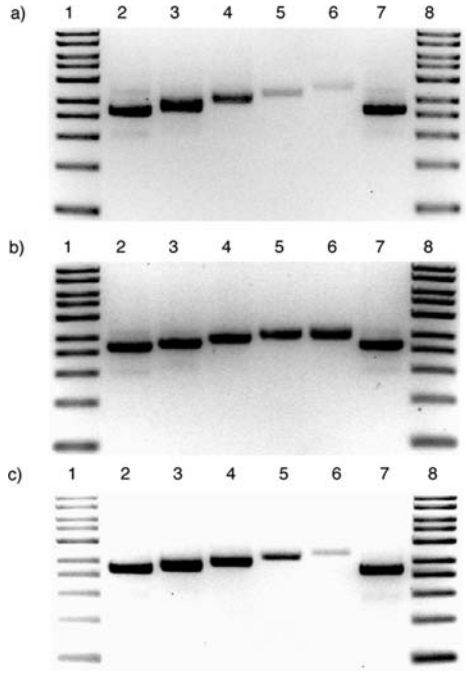

Figure 7. Imaged ethidium bromide stained agarose gel of 50 μM linearized pUC19 plasmid (10 mM phosphate buffer, pH = 8.3) irradiated with $\lambda_{irr} \geq 395$ nm in various concentrations of (a) **1** and (b) **2** (t_{irr} = 5 min). Lanes 3–6: 1, 2.5, 5, 10 μM complex. (c) **3** (t_{irr} = 15 min). Lanes 3–6: 5, 10, 25, 50 μM complex. Lanes 1 and 8, 1 kb DNA molecular weight standard; and lanes 2 and 7, linearized plasmid alone.

displays the mobility shift assay for **2** using $\lambda_{irr} \geq 645$ nm light, which shows a significant decrease in DNA mobility at complex concentrations of 1, 5, 10, and 25 μM complex with t_{irr} = 30 min. Figure S8b depicts the incubation experiment in the dark for 30 min at 298 K at the same concentrations for which there was no observed decrease in mobility.

Cell Toxicity Studies. Cellular toxicity studies were performed by monitoring HeLa cells incubated with complexes **1** and **3**; complex **2** was not investigated owing to its ~3-fold lower ligand exchange quantum yield. HeLa cells were treated with $\mathbf{1}(Cl)_2$ and $\mathbf{3}(Cl)_2$ for 2 h in the dark, followed by incubation with SYTOX Green for 10 min. SYTOX Green is a cell-permeable dye that can only translocate cells when the cell membrane has been compromised, such as those of dead or dying cells.[38] The fluorescence of SYTOX Green increases by a factor of 100 when it binds to nuclear DNA after it is internalized.[38] Cells treated with $\mathbf{1}(Cl)_2$ and $\mathbf{3}(Cl)_2$ at a concentration of 100 μM in the dark show no green fluorescence localized in the nucleus of the cell (Figure 8a,c), an indication that the compounds are not toxic in the dark as compared to the control when no complex is present. Therefore, the LC_{50} values of these complexes in the dark, $LC_{50}^{1,dark}$ and $LC_{50}^{3,dark}$, is estimated to be $\gg$100 μM. Cells treated with $\mathbf{1}(Cl)_2$ and irradiated with visible light (λ_{irr} > 400 nm) for 1 h also showed no green fluorescence, indicating that $LC_{50}^{1,irr} \gg 100$ μM (Figure 8b). Conversely, green staining was observed for $\mathbf{3}(Cl)_2$ after 1 h of irradiation (λ_{irr} > 400 nm), indicating that photoproducts from this compound damage the cell (Figure 8d). For the sake of comparison, fluorescence microscopy was also performed for the 100 μM of free 5CNU ligand (Figure 8e). It is evident from Figures 8d and 8e that significant cell death is present at 100 μM of irradiated $\mathbf{3}(Cl)_2$ and 5CNU, respectively. A concentration dependence of the toxicities of irradiated $\mathbf{3}(Cl)_2$

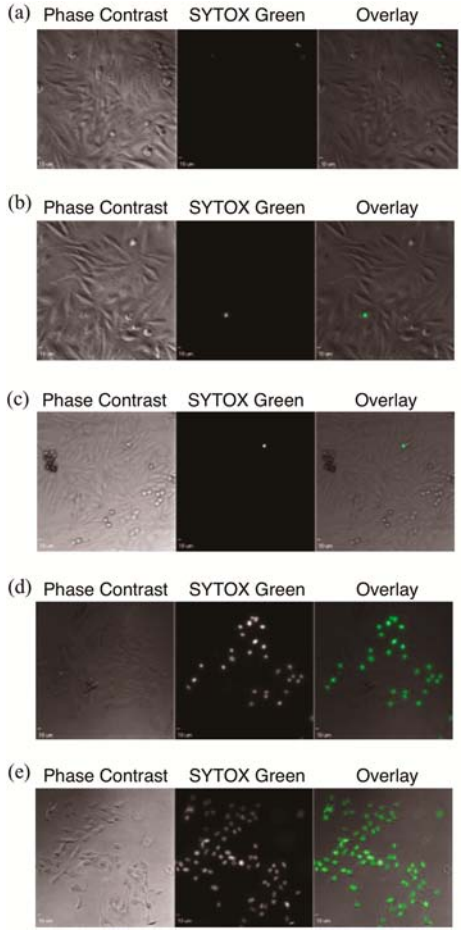

Figure 8. Fluorescence microscopy of HeLa cells incubated with 100 μM of $\mathbf{1}(Cl)_2$ (a) incubated in the dark and (b) irradiated, 100 μM of $\mathbf{3}(Cl)_2$ (c) incubated in the dark and (d) irradiated, and (e) 100 μM 5CNU alone incubated in the dark (λ_{irr} > 400 nm, t_{irr} = 1 h; dark incubation 1 h at 25 °C).

and free 5CNU (10, 20, 50, 100, and 150 μM) was used to determine the LC_{50} values, 156 ± 18 and 151 ± 33 μM, respectively. It should be noted that control experiments under similar conditions in the absence of complex, both in the dark and upon irradiation, do not result in cell death (Figure S9).

The similar toxicities of irradiated $\mathbf{3}(Cl)_2$ and free 5CNU suggest that only one 5CNU ligand is released upon irradiation under these experimental conditions. Since compound $\mathbf{1}(Cl)_2$ was found to bind to DNA *in vitro*, its lack of toxicity is likely the result of the exchange of a single CH_3CN ligand under the weaker irradiation of the cell cultures. When **2** is dissolved in aqueous media, the chloride ligand exchanges with a water molecule to generate the **Mono-aqua** species depicted in Figure 3a; this is the same molecule generated when a single ligand is exchanged photochemically from $\mathbf{1}(Cl)_2$. It is evident from the DNA binding data for **2** in the dark that the **Mono-aqua** complex does not bind to DNA (Figure S7b); therefore, the exchange of a single CH_3CN ligand in **1** is not expected to impart cellular toxicity. Inability of **1** to enter the cells or the nucleus, however, cannot be ruled out at this time. It is also possible that complex $\mathbf{3}(Cl)_2$ does not enter the cell but instead releases 1 equiv of 5CNU outside the cellular membrane upon irradiation. Current efforts are focused on elucidating the mechanism of cell death imparted by $\mathbf{3}(Cl)_2$ upon irradiation, improving the cellular penetration of the

dx.doi.org/10.1021/ja4045604 | J. Am. Chem. Soc. 2013, 135, 11274–11282

complexes and on increasing the quantum yield of ligand exchange, especially for the release of multiple ligands.

CONCLUSIONS

The data presented herein support the conclusion that **1** and **2** efficiently undergo photoinduced ligand exchange with Cl^- and H_2O, and that the new complex, **3**, also undergoes efficient exchange with H_2O. Complexes **1**−**3** exchange only the axial acetonitrile or 5CNU ligands upon irradiation. DFT calculations indicate that Ru-L(σ^*) orbitals with M-L antibonding character to the axial ligands are present in **1**−**3**, but that the respective orbitals with M-L antibonding character to the equatorial ligands are not present at low energies. The lower energy Ru-L(σ^*) orbitals are also present in the mono-aqua intermediate complexes *cis*-$[Ru(tpy)(CH_3CN)_2(H_2O)]^{2+}$ and *cis*-$[Ru(tpy)(5CNU)_2(H_2O)]^{2+}$ and are expected to aid in the exchange of the second axial ligand instead of the equatorial ligand. Complexes **1**−**3** are able to bind to DNA with $\lambda_{irr} \geq$ 395 nm, and **2** binds to DNA when irradiated with light in the PDT window. The release of one 5CNU ligand of **3** upon irradiation with visible light induces cell toxicity upon irradiation, whereas the formation of the **Mono-aqua** species from the photolysis of **1** does not affect cellular viability. Strategies are being sought to increase the ligand exchange quantum yields and the cellular penetration of these compounds.

ASSOCIATED CONTENT

Supporting Information

Emission spectra at 77 K, photolysis data, additional DNA mobility shift assays, and cytotoxicity control experiments. This material is available free of charge via the Internet at http://pubs.acs.org.

AUTHOR INFORMATION

Corresponding Author

turro@osu.edu; dunbar@mail.chem.tamu.edu

Notes

The authors declare no competing financial interest.

ACKNOWLEDGMENTS

C.T. thanks the National Science Foundation (CHE-1213646) and the Ohio Super Computer Center for partial funding. R.N.G. would like to thank National Institutes of Health, National Institute of General Medical Sciences (GM 833552). K.R.D. thanks the National Science Foundation (CHE-1213646) for support of the work performed by A.D., and Prof. J. P. Pellois for the use of his tissue culture facilities.

REFERENCES

(1) Jamieson, E. R.; Lippard, S. J. *Chem. Rev.* **1999**, *99*, 2467−2498.
(2) Antonarakis, E. S.; Emadi, A. *Cancer Chemother. Pharmacol.* **2010**, *66*, 1−9.
(3) (a) Cvitkovic, E. *Br. J. Cancer* **1998**, *77* (Suppl 4), 8−11. (b) Bleiberg, H. *Br. J. Cancer* **1998**, *77* (Suppl 4), 1−3.
(4) Wheate, N. J.; Walker, S.; Craig, G. E.; Oun, R. *Dalton Trans.* **2010**, *39*, 8113−8127.
(5) (a) Dropcho, E. J. *Semin. Neurol.* **2010**, *30*, 273−286. (b) Schmidinger, M.; Bellmunt, J. *Cancer Treat. Rev.* **2010**, *36*, 416−424. (c) Mihalcea, O.; Arnold, A. C. *Oftalmologia* **2008**, *52*, 36−40.
(6) Juarranz, A.; Jaén, P.; Sanz-Rodríguez, F.; Cuevas, J.; González, S. *Clin. Transl. Oncol.* **2008**, *10*, 148−154.
(7) Nyst, H. J.; Tan, I. B.; Stewart, F. A.; Balm, A. J. M. *Photodiagn. Photodyn. Ther.* **2009**, *6*, 3−11.
(8) O'Connor, A. E.; Gallagher, W. M.; Byrne, A. T. *Photochem. Photobiol.* **2009**, *85*, 1053−1074.
(9) Lutterman, D. A.; Fu, P. K.; Turro, C. *J. Am. Chem. Soc.* **2006**, *128*, 738−739.
(10) Singh, T. N.; Turro, C. *Inorg. Chem.* **2004**, *43*, 7260−7262.
(11) Garner, R. N.; Joyce, L. E.; Turro, C. *Inorg. Chem.* **2011**, *50*, 4384−4391.
(12) Garner, R. N.; Gallucci, J. C.; Dunbar, K. R.; Turro, C. *Inorg. Chem.* **2011**, *50*, 9213−9215.
(13) (a) Filevich, O.; Salierno, M.; Etchenique, R. *J. Inorg. Biochem.* **2010**, *104*, 1248−1251. (b) Salierno, M.; Marceca, E.; Peterka, D. S.; Yuste, R.; Etchenique, R. *J. Inorg. Biochem.* **2010**, *104*, 418−422. (c) Salierno, M.; Fameli, C.; Etchenique, R. *Eur. J. Inorg. Chem.* **2008**, 1125−1128.
(14) (a) Ostrowski, A. D.; Ford, P. C. *Dalton Trans.* **2009**, 10660−10669. (b) Ford, P. C. *Acc. Chem. Res.* **2008**, *41*, 190−200.
(15) Liu, Y.; Turner, D. B.; Singh, T. N.; Angeles-Boza, A. M.; Chouai, A.; Dunbar, K. R.; Turro, C. *J. Am. Chem. Soc.* **2009**, *131*, 26−27.
(16) Juris, A.; Balzani, V.; Barigelletti, F.; Campagna, S.; Belser, P.; von Zelewsky, A. *Coord. Chem. Rev.* **1988**, *84*, 85−277.
(17) Allison, R. R.; Sibata, C. H. *Photodiagn. Photodyn. Ther.* **2010**, *7*, 61−75.
(18) Corral, E.; Hotze, A. C. G.; Magistrato, A.; Reedijk, J. *Inorg. Chem.* **2007**, *46*, 6715−6722.
(19) Novakova, O.; Kasparkova, J.; Vrana, O.; van Vliet, P. M.; Reedijk, J.; Brabec, V. *Biochemistry* **1995**, *34*, 12369−12378.
(20) (a) Okamoto, I.; Iwamoto, K.; Watanabe, Y.; Miyake, Y.; Ono, A. *Angew. Chem., Int. Ed.* **2009**, *48*, 1648−1651. (b) Gentry, G. A.; Morse, P. A.; Dorsett, M. T. *Cancer Res.* **1971**, *31*, 909−912. (c) Porter, D. J.; Chestnut, W. G.; Merrill, B. M.; Spector, T. *J. Biol. Chem.* **1992**, *267*, 5236−5242.
(21) Longley, D. B.; Harkin, D. P.; Johnston, P. G. *Nat. Rev. Cancer* **2003**, *3*, 330−338.
(22) Sullivan, B. P.; Calvert, J. M.; Meyer, T. J. *Inorg. Chem.* **1980**, *19*, 1404−1407.
(23) Suen, H. F.; Wilson, S. W.; Pomerantz, M.; Walsh, J. L. *Inorg. Chem.* **1989**, *28*, 786−791.
(24) Montalti, M.; Credi, A.; Prodi, L.; Gandolfi, M. T. *Handbook of Photochemistry*, 3rd ed.; CRC Press: Boca Raton, FL, 2006.
(25) Sun, Y.; Lutterman, D. A.; Turro, C. *Inorg. Chem.* **2008**, *47*, 6427−6434.
(26) Frisch, M. J.; Trucks, G. W.; Schlegel, H. B.; Scuseria, G. E.; Robb, M. A.; Cheeseman, J. R.; Scalmani, G.; Barone, V.; Mennucci, B.; Petersson, G. A.; Nakatsuji, H.; Caricato, M.; Li, X.; Hratchian, H. P.; Izmaylov, A. F.; Bloino, J.; Zheng, G.; Sonnenberg, J. L.; Hada, M.; Ehara, M.; Toyota, K.; Fukuda, R.; Hasegawa, J.; Ishida, M.; Nakajima, T.; Honda, Y.; Kitao, O.; Nakai, H.; Vreven, T.; Montgomery, J. A., Jr.; Peralta, J. E.; Ogliaro, F.; Bearpark, M.; Heyd, J. J.; Brothers, E.; Kudin, K. N.; Staroverov, V. N.; Kobayashi, R.; Normand, J.; Raghavachari, K.; Rendell, A.; Burant, J. C.; Iyengar, S. S.; Tomasi, J.; Cossi, M.; Rega, N.; Millam, N. J.; Klene, M.; Knox, J. E.; Cross, J. B.; Bakken, V.; Adamo, C.; Jaramillo, J.; Gomperts, R.; Stratmann, R. E.; Yazyev, O.; Austin, A. J.; Cammi, R.; Pomelli, C.; Ochterski, J. W.; Martin, R. L.; Morokuma, K.; Zakrzewski, V. G.; Voth, G. A.; Salvador, P.; Dannenberg, J. J.; Dapprich, S.; Daniels, A. D.; Farkas, Ö.; Foresman, J. B.; Ortiz, J. V.; Cioslowski, J.; Fox, D. J. *Gaussian 09*, revision A.1; Gaussian, Inc.: Wallingford, CT, 2009.
(27) Becke, A. D. *Phys. Rev. A* **1988**, *38*, 3098−3100.
(28) Becke, A. D. *J. Chem. Phys.* **1993**, *98*, 5648−5652.
(29) Lee, C.; Yang, W.; Parr, R. G. *Phys. Rev. B: Condens. Matter Mater. Phys.* **1988**, *37*, 785−789.
(30) Hehre, W. J.; Radom, L.; Schleyer, P. V.; Pople, J. A. *Ab Initio Molecular Orbital Theory*; John Wiley & Sons: New York, 1986.
(31) Andrae, D.; Haussermann, U.; Dolg, M.; Stoll, H.; Preuss, H. *Theor. Chim. Acta* **1990**, *77*, 123−141.

(32) Dennington, R., II; Keith, T.; Millam, J. *GaussView 3*; Semichem, Inc.: Shawnee Mission, KS, 2007.
(33) (a) Lin, C.-T.; Böttcher, W.; Chou, M.; Creutz, C.; Sutin, N. *J. Am. Chem. Soc.* **1976**, *98*, 6536−6544. (b) Creutz, C.; Chou, M.; Netzel, T. L.; Okumura, M.; Sutin, N. *J. Am. Chem. Soc.* **1980**, *102*, 1309−1319.
(34) Coe, B. J.; Thompson, D. W.; Culbertson, C. T.; Schoonover, J. R.; Meyer, T. J. *Inorg. Chem.* **1995**, *34*, 3385−3395.
(35) Hutchison, K.; Morris, J. C.; Mile, T. A.; Walsh, J. L.; Thompson, D. W.; Peterson, J. D.; Schoonover, J. R. *Inorg. Chem.* **1999**, *38*, 2516−2523.
(36) Adeyemi, S. A.; Dovletoglou, A.; Guadalupe, A. R.; Meyer, T. J. *Inorg. Chem.* **1992**, *31*, 1375−1383.
(37) (a) Prussin, A. J., II; Zhao, S.; Jain, A.; Winkel, B. S. J.; Brewer, K. J. *J. Inorg. Biochem.* **2009**, *103*, 427−431. (b) Milkevitch, M.; Storrie, H.; Brauns, E.; Brewer, K. J.; Shirley, B. W. *Inorg. Chem.* **1997**, *36*, 4534−4538.
(38) *Molecular Probes: The Handbook*; Invitrogen, 2007.